Edelweiss Applied Science and Technology
ISSN: 2576-8484
Vol. 9, No. 10, 189-211
2025
Publisher: Learning Gate
DOI: 10.55214/2576-8484.v9i10.10383

Thermofusionnet for breast abnormality detection through visual and infrared thermal imaging using deep learning

Dipali Ghatge[1*], K. Rajeswari[2]
[1]Research Scholor, Pimpri Chinchwad College of Engineering, Pimpri-Chinchwad, Maharashtra, 411044, India; dipalighatge82@gmail.com (D.G.).
[2]Savitribai Phule Pune University, Pune, Maharashtra, 411007, India; kannan.rajeswari@pccoepune.org (K.R.).

Abstract: Breast cancer remains a leading cause of mortality among women worldwide, making early and accurate detection vital for effective treatment. This study proposes a deep learning model, ThermoFusionNet, which integrates visual and infrared thermal imaging to detect breast abnormalities in a cost-effective and non-invasive manner. Adaptive Bilateral Kernel Filtering (ABKF) reduces noise while preserving edges in input images. Segmentation uses Distance Regularised Level Set Evolution (DRLSE) for precise delineation of breast tissue irregularities. Feature sensitivity and segmentation convergence are enhanced by Anisotropic Gaussian Smoothing Gradient-Based Optimisation (AGSGO). Classification is performed on fused visual and thermal image data. Experimental results demonstrate characteristic fluctuations in a shared feature axis ranging from 0 to 120, where benign cases maintain values below 10, and malignant cases begin above 160, peaking before declining. Malignant features exhibit distinct thermal and visual patterns that aid reliable detection. The model achieves improved accuracy and sensitivity compared to traditional methods. These findings support ThermoFusionNet as an effective diagnostic tool for early breast cancer detection. Future work aims at real-time diagnostics and mobile health integration to increase accessibility in low-resource settings.

Keywords: *Adaptive bilateral kernel filtering, anisotropic Gaussian smoothing, breast cancer, distance-regularized level set evolution, gradient-based optimization, thermal imaging, ThermoFusionNet*

1. Introduction

Breast cancer detection has long been an experiment in medical imaging, with progress being made over the centuries to improve the precision and dependability of analytic tools [1]. Traditionally, mammography and ultrasound have been the gold standards for early detection. However, these methods often face limitations such as false positives, discomfort during procedures, and challenges in detecting abnormalities in dense breast tissue [2]. In the past, these diagnostic techniques relied heavily on physical examinations by radiologists, which not only resulted in lengthy diagnoses but also produced unpredictable results [3]. While mammography has been the leading tool in the discovery of breast abnormalities, it exposes patients to ionizing energy, which poses risks, chiefly for older women or those with a hereditary disposition to breast cancer [4]. These issues highlight the urgent need for more advanced, non-invasive diagnostic methods that can detect breast irregularities with greater accuracy and lower risks [5]. As a result, infrared current imaging occurred as a budding resolution due to its non-invasive nature, the non-appearance of energy, and its aptitude to detect infection differences produced by irregular tissue growth [6-8]. Thermal imaging has been investigated in the past as a promising technique to identify infection changes in breast tissue, but understanding this data precisely has posed a significant challenge due to the difficulties involved in analyzing infrared images [9-11].

The arrival of DL and AI has revolutionized the probability of medical imaging, allowing for the programmed and precise analysis of composite data, such as ultraviolet thermal images [12-14].

History: Received: 15 August 2025; Revised: 8 September 2025; Accepted: 12 September 2025; Published: 7 October 2025
* Correspondence: dipalighatge82@gmail.com

ThermoFusionNet, a groundbreaking deep learning-based method, has been introduced to address the problem of accurately detecting breast abnormalities using both visual and infrared thermal images [15-17]. The motivation behind this research is to create a system that not only overcomes the limitations of traditional diagnostic methods but also ensures quicker, more reliable, and less invasive breast cancer detection [18, 19]. The upcoming possibility of ThermoFusionNet includes its addition to technical research, where it can be used as a complementary analytic tool to assist radiologists and registrars in identifying breast irregularities at the earliest stages [20-22]. ThermoFusionNet offers an exciting frontier in breast tumour discovery, combining the power of deep learning and non-invasive thermal imaging to create a more reliable, accessible, and efficient analytic instrument for the future [23, 24]. The remaining sections are decided as follows: The literature review was described in Section 2, the proposed technique was labeled in Section 3, the results were discussed in Section 4, and the paper's conclusion was described in Section 5.

2. Literature Survey

The literature survey identifies existing approaches for breast abnormality recognition using graphic and ultraviolet thermal imaging, focusing on deep learning advancements such as ThermoFusionNet for improved accuracy and early diagnosis. Jalloul et al. [25] early detection is central, predominantly for females, as old-style broadcast approaches like mammography often struggle with correctness in cases of impenetrable breast tissue. The maximum demonstration, accomplishing 97.62% accuracy, 95.79% precision, 98.53% recall, 94.52% specificity, an F1 score of 97.16%, an area under the curve (AUC) of 99%, a latency of 0.06 s, and CPU utilization of 88.66%. To perceptively improve the accuracy and capability of breast growth detection, subordinate its character as a valuable apparatus for early decision. Al Husaini et al. [26] add to the breast cancer group correctness by preserving spatial features and leveraging the in situ cooling provision. This study's exercise dataset comprised 1000 thermal images; the current camera related to a mobile expedient was rummage sale for the imaging procedure. The findings maintain the efficiency of beginning for actual breast growth discovery, especially when collected with in situ refrigeration gel and variable tumour infections. Ahmed et al. [27] breast cancer discovery at an initial phase is crucial for educating patients about survival rates. The logistic regression presented an outstanding performance, attaining a correctness of 0.976, an F1 score of 0.977, an accuracy of 1.000, and a recall of 0.995. This indicates a high level of accuracy in correctly categorizing current irregularities connected with breast tumours. Mirasbekov et al. [28] breast cancer remains a global health problem requiring effective diagnostic approaches for early discovery. The World Health Organization's ultimate goal of breast self-examination is supported by advancements in thermal imaging combined with explainable artificial intelligence and medical records. This integrated approach achieved a correctness of 84.07%, while model B, which also includes a CNN forecast, attained a correctness of 90.93%. Khan et al. emphasize that breast cancer continues to be one of the most recurrent and serious cancers in women worldwide, highlighting the need for more accurate diagnostics in its initial stages to improve rehabilitation efficiency and survival rates.

Khomsi et al. [29] breast cancer judgment: tumour size is key to improving the patient's survival chances. The prediction accuracy indicates the volume of the planned FF-DNN model to approximate tumour scope from the provided relevant features, with an MSE value of 0.194 and an R2 value of 0.998. Bani Ahmad et al. [30] thermography is a less aggressive and reasonable method that is becoming increasingly popular. In light of this, a recent deep learning (DL)-based breast cancer analysis method is performed using thermography images. The thermography images are selected from connected details. Pechkova et al. [31] proposed a progressive approach to investigate thermal descriptions for breast cancer recognition employing machine learning methods. Ukiwe et al. [32] DL models have been developed popular for identifying irregularities in corporeal and organic schemes, by the instrumentality of image elimination of images in CNN. Munguía-Siu et al. [33] breast cancer is one of the foremost causes of death for women worldwide, and early detection can help reduce the mortality rate. The best presentation for visualizing breast tumors was VGG16-LSTM, which demonstrated an accuracy,

Edelweiss Applied Science and Technology
ISSN: 2576-8484
Vol. 9, No. 10: 189-211, 2025
DOI: 10.55214/2576-8484.v9i10.10383

sensitivity, and specificity of 95.72% and 98.68%, respectively. That chronological data retrieval from energetic breast thermography is conceivable without meaningful cooperation of classifier runtime.

3. Research Proposed Methodology

The future practice for ThermoFusionNet involves a deep learning-based framework that integrates both visual and infrared thermal images to enhance the discovery of breast abnormalities. The process begins with data acquisition, collecting synchronized visual and thermal images of the breast. These images are then pre-processed to normalize contrast, align modalities, and remove noise. Feature extraction is performed using neural networks tailored to each modality. A fusion layer combines extracted features from both visual and thermal domains, allowing the system to study complementary patterns. The fused features are then passed through classification layers for identifying standard and irregular breast tissues. The model is trained and validated using annotated datasets, ensuring robustness and high accuracy in real-world diagnostic scenarios.

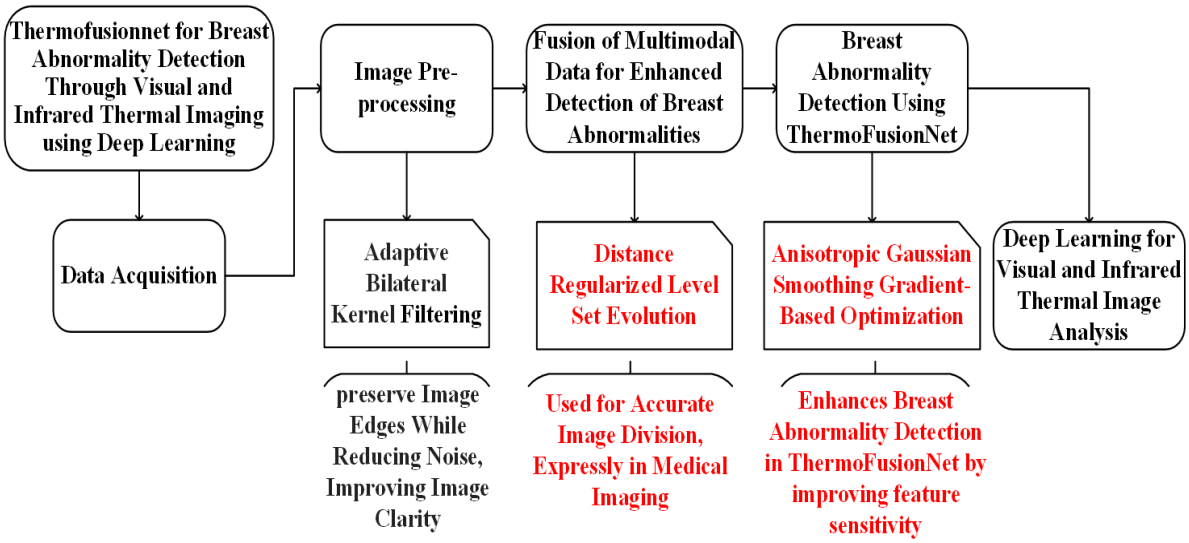

Figure 1.
Block Diagram of the Proposed Work.

Figure 1 illustrates the comprehensive pipeline for breast abnormality detection through integrated visual and infrared thermal imaging using deep learning. It begins with data acquisition, where RGB and infrared thermal images are collected from clinical and public datasets in the Breast Thermography Dataset. In the image pre-processing stage, images are resized, denoised using Adaptive Bilateral Kernel Filtering, aligned, and augmented to ensure consistency and diversity. The data fusion combines anatomical visual and physiological thermal information, enhanced by distance-regularized level set evolution. The abnormality detection module employs anisotropic Gaussian smoothing gradient-based optimization to model visual-thermal relationships. The deep learning analysis utilizes Spiking Neural Networks with Neural Architecture Search for the adaptive and accurate discovery of breast irregularities in real-time.

3.1. Image Acquisition

Image acquisition for ThermoFusionNet involves collecting both visual and infrared thermal images of the breast from diverse sources, including clinical datasets, publicly available breast imaging databases, and real-time imaging systems. The Breast Thermography Dataset is referenced from Mendeley Data. This dataset contains thermographic images of the female thorax, captured using a

Edelweiss Applied Science and Technology
ISSN: 2576-8484
Vol. 9, No. 10: 189-211, 2025
DOI: 10.55214/2576-8484.v9i10.10383

FLIR A300 camera, featuring both benign and malignant cases for training breast abnormality detection models. Visual descriptions are obtained using average RGB cameras, while infrared thermal descriptions are acquired using thermal imaging cameras, such as FLIR or comparable devices. These images are then pre-processed to ensure uniformity in size, clarity, and configuration for effective fusion. A comprehensive dataset, encompassing both standard and atypical cases, is essential for training deep learning models, ensuring accurate and reliable detection of breast abnormalities.

Figure 2.
Thermal Camera Used FLIR E5-X Object.

Figure 2 shows the thermal camera used by FLIR E5-X. The object highlights the advanced thermal imaging device employed for capturing breast thermograms. The FLIR E5-X is a high-resolution infrared camera designed to detect and visualize temperature differences with precision. Its sensitive thermal sensor captures detailed heat patterns on the skin surface, which are crucial for identifying abnormal temperature variations associated with breast abnormalities. Compact and user-friendly, the FLIR E5-X provides accurate, non-invasive imaging, making it ideal for medical diagnostics. The captured thermal images serve as essential input data for analysis using AI models like ThermoFusionNet, enhancing early detection and diagnosis.

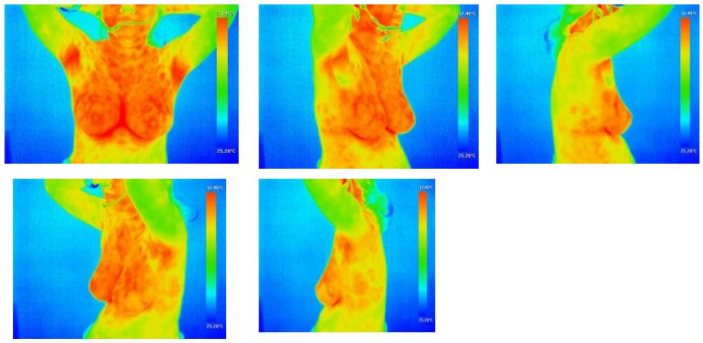

Figure 3.
Breast thermogram captured from five different positions.

Figure 3 illustrates thermal images of the breast taken from multiple angles, typically front, left 45°, right 45°, left lateral, and right lateral views. This multi-angle approach ensures comprehensive thermal mapping of the breast region, enabling better visualization of temperature variations that may indicate

Edelweiss Applied Science and Technology
ISSN: 2576-8484
Vol. 9, No. 10: 189-211, 2025
DOI: 10.55214/2576-8484.v9i10.10383

abnormalities. By capturing thermograms from different positions, clinicians can detect asymmetries or localized hot spots that may not be visible in a single view. This technique enhances diagnostic accuracy in early breast abnormality detection and supports more reliable assessment when using AI-based models like ThermoFusionNet.

3.2. Image Pre-Processing

Pre-processing for ThermoFusionNet involves several critical steps to ensure high-quality input for the DL model. The visual and infrared thermal images are resized to a reliable resolution to ensure uniformity. Adaptive Bilateral Kernel Filtering (ABKF) assists in preserving duplicate boundaries while reducing noise, enhancing image clarity for both graphic and ultraviolet thermal images, thereby improving ornamental feature abstraction and model accuracy. Both image types undergo normalization to standardize pixel values, which enhances model performance during training. Image alignment is performed to match corresponding visual and thermal images, ensuring accurate fusion. Data augmentation techniques, such as rotation, flipping, and scaling, are employed to increase dataset diversity and prevent overfitting. Noise reduction methods are also utilized to recover image clarity and improve feature extraction.

3.2.1. Feature Extraction

Feature extraction in ThermoFusionNet involves identifying and isolating key patterns from visual and infrared thermal images, which are crucial for accurately detecting breast abnormalities. The process begins with pre-processed images that are resized, normalized, and aligned, ensuring consistency across both image types. Adaptive Bilateral Kernel Filtering (ABKF) enhances image clarity by removing noise while preserving important edges, making subtle irregularities more noticeable. Once the images are pre-processed, feature extraction focuses on capturing distinctive characteristics like texture, shape, and edge details from both visual and thermal data. These features are then used by the deep learning model to differentiate between normal and abnormal tissue patterns. Techniques such as edge detection, histogram analysis, and texture-based methods are often employed to extract relevant features. By leveraging the fusion of both visual and thermal information, feature extraction aids the model in making precise predictions, improving the detection of benign and malignant cases in breast thermography images.

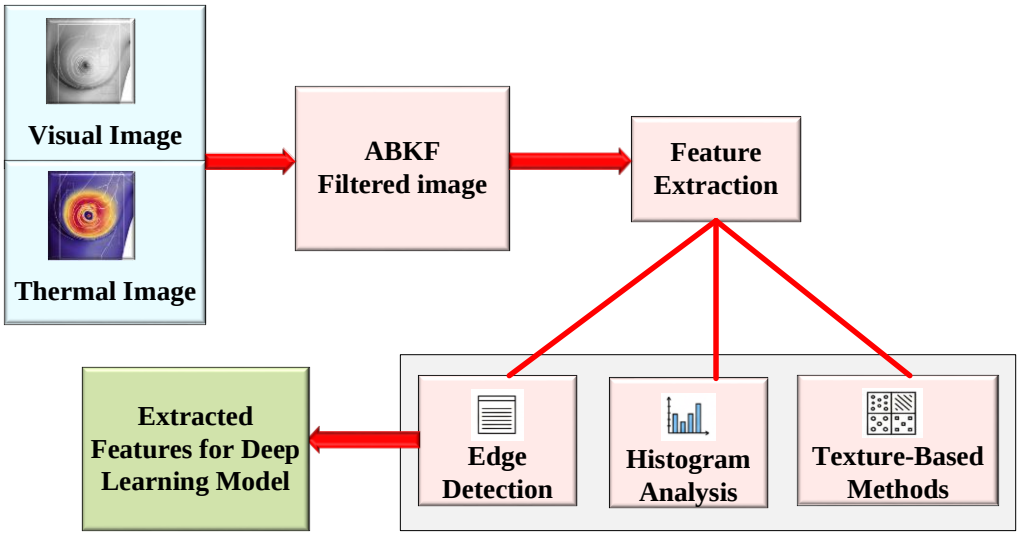

Figure 4.
Image Pre-Processing Module.

Edelweiss Applied Science and Technology
ISSN: 2576-8484
Vol. 9, No. 10: 189-211, 2025
DOI: 10.55214/2576-8484.v9i10.10383

Figure 4 shows that the image pre-processing module enhances raw input images to improve the accuracy and efficiency of subsequent image analysis tasks. This module typically includes steps such as noise reduction using filters, contrast enhancement to highlight important features, and normalization to standardize image intensity values. Additional operations may involve resizing, grayscale conversion, and edge enhancement to simplify feature extraction. These steps collectively ensure that the input image is clean, consistent, and optimized for segmentation or classification. The module plays a vital role in improving the robustness of the system by minimizing variations and distortions in the raw data before advanced processing begins.

3.2.2. Adaptive Bilateral Kernel Filtering (ABKF)

Adaptive Bilateral Kernel Filtering (ABKF) enhances the ThermoFusionNet deep learning model used for breast abnormality detection via both pictorial and ultraviolet thermal imaging. ABKF addresses noise and artifacts in breast thermography images caused by device limitations, patient variations, and environmental factors. By selectively smoothing areas without blurring critical edges, ABKF ensures important diagnostic features are preserved, improving image quality. This results in better feature extraction for the deep learning model, enhancing its ability to distinguish between normal and abnormal tissue. ABKF improves the fusion of visual and thermal data, making subtle irregularities more detectable and boosting diagnostic accuracy. The ABKF reckoning is typically articulated as:

$$I_{filtered}(x) = \frac{1}{W(x)} \sum_{x_i \in \Omega} I(x_i) \cdot f_s(\| x - x_i \|) \cdot f_r(| I(x) - I(x_i) |) \cdot a(x, x_i) \qquad (1)$$

Where $I(x)$ Original pixel intensity at position x, Ω is the neighbourhood around pixel x, f_s is a Spatial Gaussian kernel (depends on pixel distance), f_r Range Gaussian kernel (depends on intensity difference). $a(x, x_i)$ Adaptation function modifies the kernel based on local texture or edge strength. $W(x)$ is the normalisation factor:

$$W(x) = \sum_{x_i \in \Omega} f_s(\| x - x_i \|) \cdot f_r(| I(x) - I(x_i) |) \cdot a(x, x_i) \qquad (2)$$

In ABKF, the adaptation function $a(x, x_i)$ dynamically adjusts the influence of neighboring pixels based on local characteristics such as gradient magnitude or edge strength. This allows better noise reduction in flat regions while protecting edges, which is dangerous for thermal and visual image fusion. By integrating ABKF in the pre-processing stage, ThermoFusionNet gains clearer, more consistent input, which improves feature extraction and boosts deep-learning model performance.

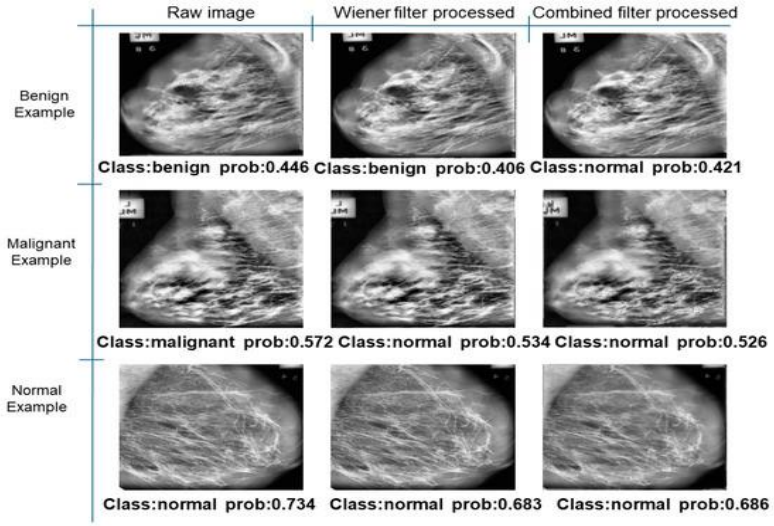

Figure 5.
Early Breast Cancer Detection.

Edelweiss Applied Science and Technology
ISSN: 2576-8484
Vol. 9, No. 10: 189-211, 2025
DOI: 10.55214/2576-8484.v9i10.10383

Figure 5 illustrates key methods and visual indicators used in the early detection of breast cancer. It may include visuals such as mammogram scans, which are standard screening tools for identifying abnormal lumps or tissue changes before symptoms appear. Areas of concern often highlighted include masses, calcifications, and asymmetries in breast tissue. The figure may also depict the breast self-examination process, educating individuals on how to detect unusual changes such as lumps, dimpling, or alterations in skin texture. Additionally, infographics might present recommended screening timelines, particularly for women over 40 or those with a family history of breast cancer. The primary goal of this figure is to promote awareness, encourage regular check-ups, and ultimately improve survival rates by facilitating early diagnosis when treatment is most effective.

3.3. Fusion of Data for Enhanced Discovery of Breast Irregularities

Fusion of data is a key component in ThermoFusionNet for enhancing breast abnormality detection. By combining visual (RGB) and infrared thermal images, the model leverages complementary information from both modalities. Visual images provide detailed anatomical structure, while thermal images highlight temperature variations associated with abnormal tissue. Distance Regularized Level Set Evolution (DRLSE) is used for accurate image segmentation, especially in medical imaging, object boundary detection, tumour localisation, and handling complex shapes without reinitialization. The fusion process can be performed at different stages: early fusion, where both image types are combined before feeding into the model, or late fusion, where each modality and its features are merged later. This fusion approach enables ThermoFusionNet to improve detection accuracy and sensitivity in identifying breast abnormalities.

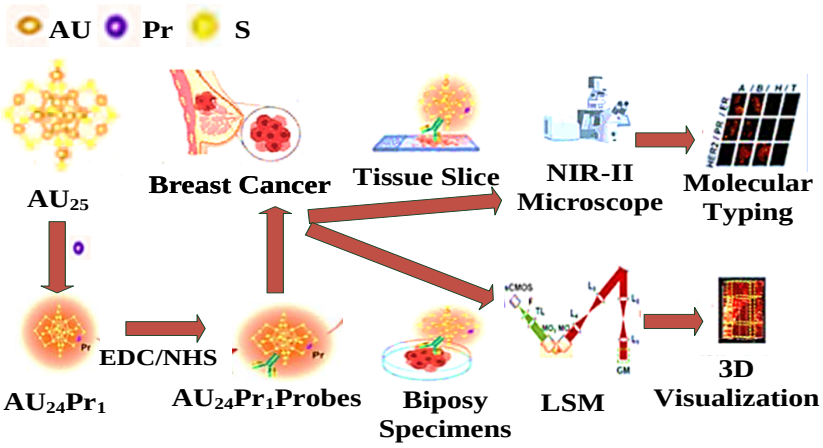

Figure 6.
Breast Cancer Pathology Evolution in Clinical Patient Tissues.

Figure 6 illustrates the pathological evolution of breast cancer in clinical patient tissues, depicting the progression from normal breast cells to malignant carcinoma. The sequence typically begins with normal ductal or lobular cells, followed by stages such as hyperplasia, atypical hyperplasia, carcinoma in situ, and finally invasive carcinoma. The figure may include histological slides stained with hematoxylin and eosin (H&E) or immunohistochemistry (IHC) to highlight cellular and molecular changes such as increased cell proliferation, nuclear atypia, and disruption of normal tissue architecture. Also, biomarker expression may be shown at different stages, providing insights into tumor biology and informing treatment decisions. These visualizations are essential for understanding breast cancer development and progression, supporting accurate diagnosis, clinical staging, and personalized therapy in medical practice.

Edelweiss Applied Science and Technology
ISSN: 2576-8484
Vol. 9, No. 10: 189-211, 2025
DOI: 10.55214/2576-8484.v9i10.10383

3.3.1. Distance Regularized Level Set Evolution (DRLSE)

DRLSE is an advanced image segmentation technique based on the level set method, which is commonly used to detect object boundaries in images. Traditional level set methods require a reinitialization step to maintain the signed distance function property of the level set function. This step ensures numerical stability during contour evolution but adds computational complexity and can introduce inaccuracies. DRLSE improves on this by introducing a distance regularization term into the level-set formulation. This term naturally maintains the level set function as a signed distance function throughout the evolution process. As a result, reinitialization is no longer necessary, which simplifies computation and enhances stability.

Distance Regularised Level Set Evolution (DRLSE) is a sophisticated mathematical model developed for image segmentation, particularly effective in delineating object boundaries within images. Unlike traditional level set methods, which require reinitialization to maintain the level set function as a signed distance function, DRLSE incorporates a distance regularization term that inherently preserves this property throughout the evolution process. This innovation eliminates the need for reinitialization, a computationally expensive and numerically delicate step that is typically necessary for conventional level set techniques to prevent instability and maintain the shape of the evolving contour. By introducing this regularization term, DRLSE ensures that the evolving level set function remains stable and well-behaved, enabling more efficient and accurate segmentation results.

Distance Regularized Level Set Evolution (DRLSE) is a mathematical model for image segmentation, particularly effective in preserving the accuracy and stability of evolving contours in images without the need for initialization. Let the evolving contour be represented implicitly by a level set function $\phi(x, y)$ where the zero level set $\phi(x, y) = 0$ defines the object boundary. The total energy functional in DRLSE is defined as:

$$E(\phi) = \mu R_p(\phi) + \lambda L_g(\phi) + \alpha A_g(\phi) \quad (3)$$

Where, $R_p(\phi)$ Distance regularization term. $L_g(\phi)$ is a length term that encourages contour alignment with object boundaries. $A_g(\phi)$ It is an Area term that speeds up contour evolution toward or away from object boundaries. μ, λ, α are Positive weighting coefficients g Edge indicator function derived from the image. Distance regularisation term $R_p(\phi)$

$$R_p(\phi) = \int_\Omega P(|\nabla\phi|)dx \quad (4)$$

Where $p(s)$ is a potential function, typically chosen such that it has a minimum at $s = 1$, encouraging ϕ to maintain $|\nabla\phi| = 1$ (i.e., the signed distance property). This term regularises the level set and avoids reinitialization. Length Term $L_g(\phi)$

$$L_g(\phi) = \int_\Omega g\delta(\phi)|\nabla\phi|dx \quad (5)$$

Drives the zero-level set toward image edges. $\delta(\phi)$ Dirac delta function localized around the zero level set. Area term $A_g(\phi)$

$$A_g(\phi) = \int_\Omega g\, H(\phi)dx \quad (6)$$

Where $H(\phi)$ is the Heavisine function that helps push or pull the contour inside or outside the target region based on the sign of α. The gradient descent flow (Euler–Lagrange equation) for minimising the energy $E(\phi)$ gives the level set evolution:

$$\frac{\partial\phi}{\partial t} = \mu\left(\Delta\phi - div\left(\frac{\nabla\phi}{|\nabla\phi|}\right)\right) + \lambda\delta(\phi)div\left(g\,\frac{\nabla\phi}{|\nabla\phi|}\right) + \alpha g\delta(\phi) \quad (7)$$

The first term of regularization is maintaining the signed distance property. The second term, edge attraction, moves the contour toward object boundaries. The third term, balloon force, controls expansion/shrinkage.

One of the primary advantages of DRLSE is its ability to produce efficient and reliable contour evolution. The method improves the precision of boundary detection and adapts effectively to complex object shapes and fine details within images. This makes it particularly suitable for applications where

Edelweiss Applied Science and Technology
ISSN: 2576-8484
Vol. 9, No. 10: 189-211, 2025
DOI: 10.55214/2576-8484.v9i10.10383

high segmentation accuracy is critical. Another key benefit is the reduction in computational complexity. Traditional level set methods often involve frequent reinitialization, which increases processing time and can degrade accuracy. DRLSE bypasses this entirely, streamlining the segmentation process and making it more robust for real-world applications. Due to its accuracy, efficiency, and stability, DRLSE is widely applied in various fields, most notably in medical imaging. It is especially valuable in tasks such as tumour boundary detection in MRI and CT scans, where the ability to handle irregular, intricate shapes is crucial. Its robustness against noise and adaptability to various image types further enhance its versatility. DRLSE represents a significant advancement in image segmentation technology, combining mathematical rigour with practical utility to solve complex imaging problems more effectively.

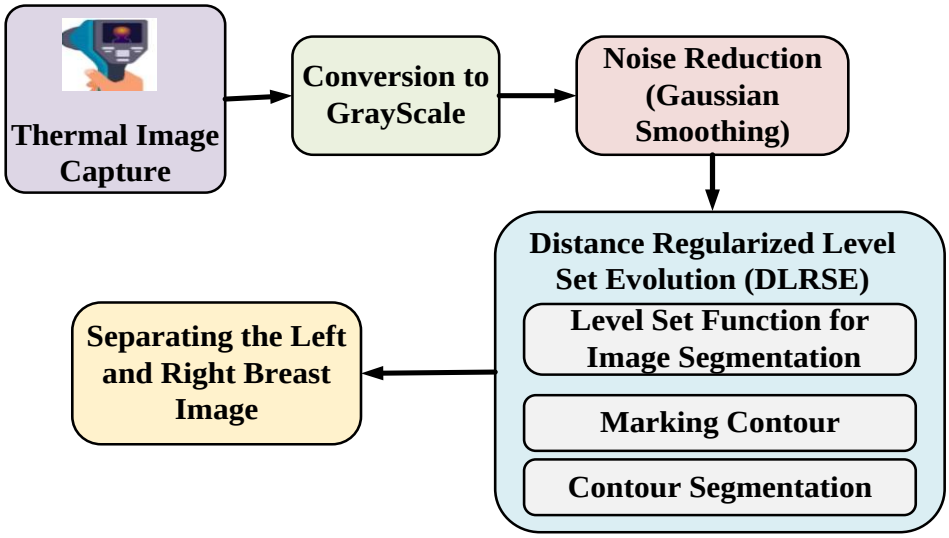

Figure 7.
Thermal Image Capture.

Figure 7 illustrates the thermal imaging process used in breast abnormality detection. An infrared thermal camera is positioned to scan the breast area, detecting infrared radiation naturally emitted by the body as heat. This non-invasive imaging technique maps temperature variations on the skin's surface, which can indicate underlying abnormalities such as tumors or inflammation. Since abnormal tissues often have higher metabolic activity, they emit more heat, resulting in localized temperature differences that the thermal camera detects. The captured thermal images provide valuable functional information that complements structural imaging methods like mammography or ultrasound. The controlled environment minimizes external temperature influences, ensuring accurate readings. This process forms the foundational step in ThermoFusionNet by supplying thermal data critical for detecting breast abnormalities.

Edelweiss Applied Science and Technology
ISSN: 2576-8484
Vol. 9, No. 10: 189-211, 2025
DOI: 10.55214/2576-8484.v9i10.10383

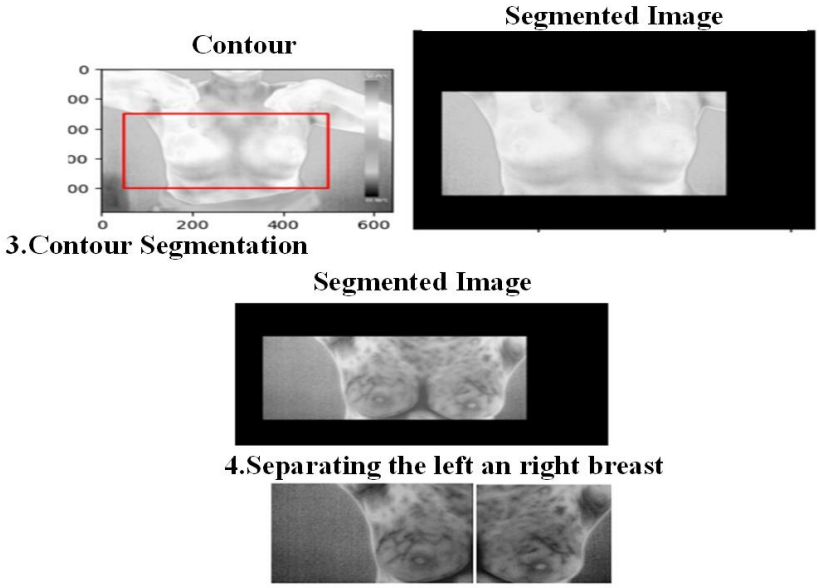

Figure 8.
Contour Segmentation and Segmented Image.

Figure 8 illustrates the contour segmentation process applied to thermal images for breast abnormality detection. The original thermal image undergoes pre-processing to enhance contrast and highlight regions of interest. The contour segmentation algorithm then identifies and traces the boundaries of distinct thermal patterns, isolating areas that may correspond to abnormal heat signatures indicative of tumours or inflammation. The resulting segmented image delineates these regions with precise contour lines, separating abnormal zones from healthy tissue. This segmentation is crucial for focusing the analysis on potential abnormalities and reducing noise from irrelevant areas. ThermoFusionNet accurately extracts features related to breast abnormalities, improving detection performance. This refines raw thermal data into actionable information for effective diagnosis.

3.4. Breast Abnormality Detection Using ThermoFusionNet

Breast abnormality detection using ThermoFusionNet involves applying deep learning to analyze visual and infrared thermal images. The model processes visual images to capture detailed anatomical features and uses current images to notice subtle temperature variations that may indicate abnormalities such as tumors or cysts. Anisotropic Gaussian Smoothing Gradient-Based Optimization (AGSGO) enhances breast abnormality detection in ThermoFusionNet by improving feature sensitivity, suppressing noise, and accelerating convergence for accurate, efficient thermal image segmentation. ThermoFusionNet combines these two modalities through data fusion techniques, allowing the model to utilize complementary information for more accurate and reliable detection. By training on a large dataset of labeled images, the model learns to distinguish between normal and abnormal tissues, enabling early discovery of breast abnormalities in a non-invasive, cost-effective manner.

3.4.1. Anisotropic Gaussian Smoothing Gradient-Based Optimisation (AGSGO)

The term Anisotropic Gaussian Smoothing Gradient-Based Optimisation (AGSGO) is not recognized in established literature. However, there is a concept known as Anisotropic Gaussian Smoothing for Gradient-Based Optimisation. This method enhances traditional gradient-based optimisation algorithms by applying anisotropic Gaussian smoothing to the gradient estimates, aiming to improve convergence and avoid suboptimal local minima. The primary goal of this approach is to replace the standard gradient with a non-local gradient derived from averaging function values using anisotropic Gaussian smoothing. Unlike isotropic Gaussian smoothing, which applies uniform smoothing in all directions, anisotropic smoothing adapts the smoothing directionality

Edelweiss Applied Science and Technology
ISSN: 2576-8484
Vol. 9, No. 10: 189-211, 2025
DOI: 10.55214/2576-8484.v9i10.10383

based on the properties of the underlying function. This adaptation is achieved by adjusting the covariance matrix of the Gaussian distribution, allowing for directional smoothing tailored to the gradient's behaviour. Let $f: R^n \to R$ be the objective function to be minimised. The standard gradient descent update rule is:

$$X_{K+1} = X_k - \eta \nabla f(x_k) \quad (8)$$

Where η is the learning rate. In Anisotropic Gaussian Smoothing Gradient Descent (AGS-GD), the gradient is replaced by a smoothed version.

While the specific application of AGSGO in ThermoFusionNet for breast abnormality detection is not detailed in the available literature, the integration of anisotropic Gaussian smoothing in gradient-based optimisation methods can be beneficial in medical imaging tasks. In such contexts, anisotropic smoothing can enhance the optimisation process by providing more accurate gradient estimates, leading to improved convergence and better detection of abnormalities in medical images.

ThermoFusionNet leverages multimodal imaging data, primarily thermal images fused with other diagnostic modalities, to enhance the accuracy and reliability of detecting anomalies such as tumours. A critical component of training this deep learning model effectively is the optimisation algorithm used to minimise the loss function, which directly impacts the model's performance. Traditional gradient-based optimisation methods often struggle with the complex, high-dimensional, and non-convex nature of deep neural network loss landscapes. These landscapes can be noisy, contain numerous local minima, and present saddle points that impede efficient convergence. To address these challenges, the Anisotropic Gaussian Smoothing Gradient-Based Optimisation (AGSGO) technique is employed. AGSGO improves gradient-based optimisation by incorporating anisotropic Gaussian smoothing into the gradient computation. Unlike isotropic smoothing, which uniformly smooths the gradient in all directions, anisotropic smoothing adapts the smoothing effect directionally, guided by the local geometry of the loss surface.

This approach allows the optimizer to selectively smooth noisy or unstable gradient components while preserving essential directional information necessary for effective descent. By applying a covariance matrix tailored to the gradient's behavior, AGSGO generates a more stable and reliable gradient estimate, leading to smoother updates during training. This directional smoothing reduces the impact of noisy fluctuations inherent in thermal imaging data and helps the network avoid shallow local minima and saddle points. Consequently, ThermoFusionNet trained with AGSGO exhibits improved convergence speed, enhanced robustness to noisy input, and better generalization in breast abnormality detection tasks. In summary, AGSGO serves as a sophisticated optimization strategy that refines the gradient signals feeding into ThermoFusionNet, enabling it to more accurately identify subtle abnormalities in breast tissue through effective fusion of thermal imaging data.

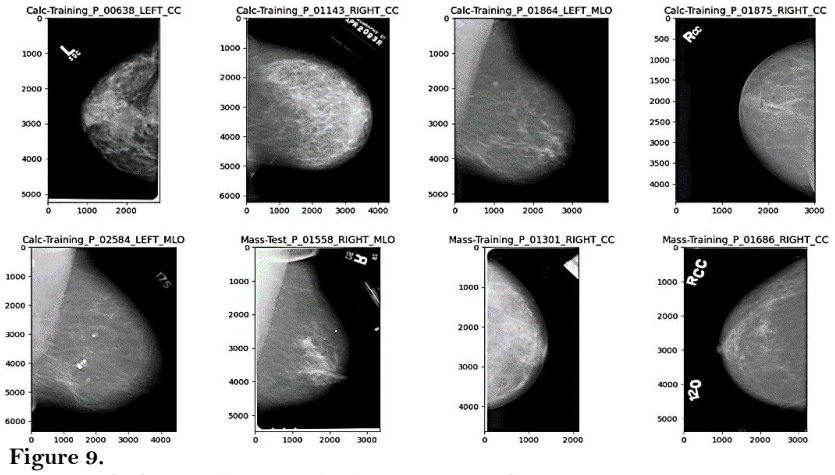

Figure 9.
Automated Abnormality Detection in Mammography.

Edelweiss Applied Science and Technology
ISSN: 2576-8484
Vol. 9, No. 10: 189-211, 2025
DOI: 10.55214/2576-8484.v9i10.10383

Figure 9 demonstrates that automated abnormality detection in mammography typically illustrates how AI and machine learning algorithms assist in identifying potential signs of breast cancer. It may display a digital mammogram with highlighted regions such as masses, microcalcifications, or architectural distortions marked by the system for further review. These areas are often outlined or colour-coded to indicate the level of suspicion. The image might also show a comparison between AI-assisted and manual readings, demonstrating improved accuracy and reduced oversight. Such visual content emphasises the role of technology in enhancing early detection, supporting radiologists, and streamlining the diagnostic workflow in clinical settings, ultimately aiming to improve patient outcomes and reduce diagnostic errors.

3.5. Deep Learning for Visual and Infrared Thermal Image Analysis

Deep learning for visual and infrared thermal image analysis in ThermoFusionNet leverages, enhancing ThermoFusionNet by efficiently processing visual and infrared thermal images, enabling accurate, real-time discovery of breast irregularities through adaptive learning, to process and analyse both visual and thermal images of the breast. The model studies classify complex patterns and features that are indicative of abnormalities, such as tumours or inflammation, from both image modalities. Visual images offer detailed anatomical context, while infrared thermal images highlight infection vicissitudes related to abnormal tissue. By combining these complementary inputs, the DL model improves detection accuracy, enabling more reliable and early identification of breast abnormalities in a non-invasive, efficient manner.

3.5.1. Classification Module

The classification module in ThermoFusionNet accurately detects breast abnormalities by leveraging both visual and infrared thermal imaging. After the pre-processing and feature extraction stages, the deep learning model utilises a neural network architecture to process the fused data. The model is trained on a diverse dataset containing both benign and malignant cases, ensuring it learns to distinguish between normal and abnormal tissue patterns. During training, the network learns to recognise complex features from both visual and thermal images, such as textures, shapes, and subtle temperature variations indicative of abnormalities. The classification module outputs predictions on whether the breast tissue is benign or malignant based on these learned patterns. The model's ability to integrate data enables more accurate decision-making, enhancing its diagnostic performance by identifying subtle abnormalities that may be missed using a single imaging modality alone.

4. Experimentation and Result Discussion

The experimentation for ThermoFusionNet was conducted using an openly obtainable dataset comprising paired visual and infrared thermal breast images. The dataset was divided into training, validation, and testing sets to evaluate the model's performance. Various metrics such as correctness, accuracy, recall, F1-score, and AUC-ROC were used for performance assessment. ThermoFusionNet demonstrated superior results compared to single-modality models, with significant improvements in detection accuracy and reduced false positives. The fusion of thermal and visual features enabled the network to better differentiate between normal and abnormal tissue patterns. Comparative experiments with traditional neural networks and unimodal models validated the effectiveness of the fusion strategy. The results confirm the potential of ThermoFusionNet as a reliable and efficient tool for initial breast abnormality detection.

Edelweiss Applied Science and Technology
ISSN: 2576-8484
Vol. 9, No. 10: 189-211, 2025
DOI: 10.55214/2576-8484.v9i10.10383

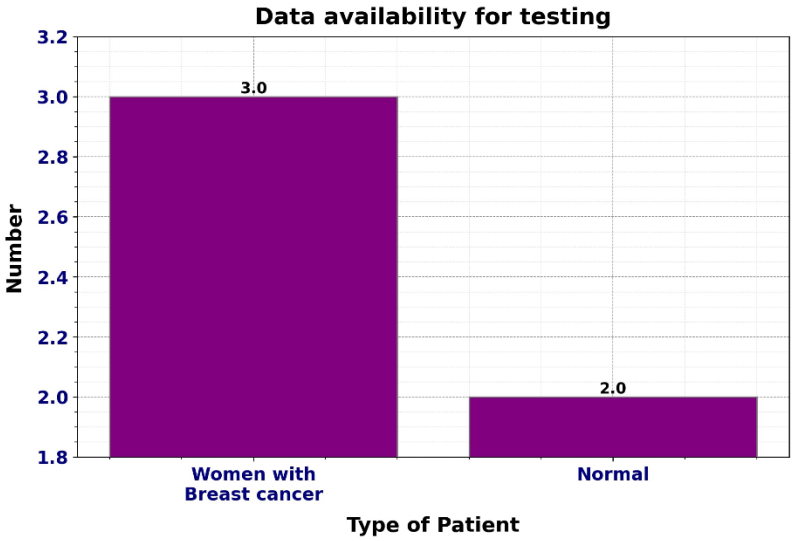

Figure 10.
The Data Availability Information for Testing.

Figure 10 represents the availability of information for testing, specifically focusing on patients categorized by type. The primary dataset reflects values about women diagnosed with normal breast cancer. The values range from 2.0 to 3.0, suggesting an evaluation of varying parameters linked to these patients. The data fluctuates among different categories within this context, indicating potential trends or relevant insights into patient outcomes and accessibility related to the testing discussed. The information could be vital for further research or understanding of breast cancer in women. While specific words relating to axes are not detailed here, it is evident that a comprehensive examination of this has significant implications for medical professionals and researchers engaged in studies concerning breast cancer awareness and treatment accessibility for women diagnosed with normal forms of this condition. This representation aims at enhancing knowledge around patient demographics and their respective health scenarios.

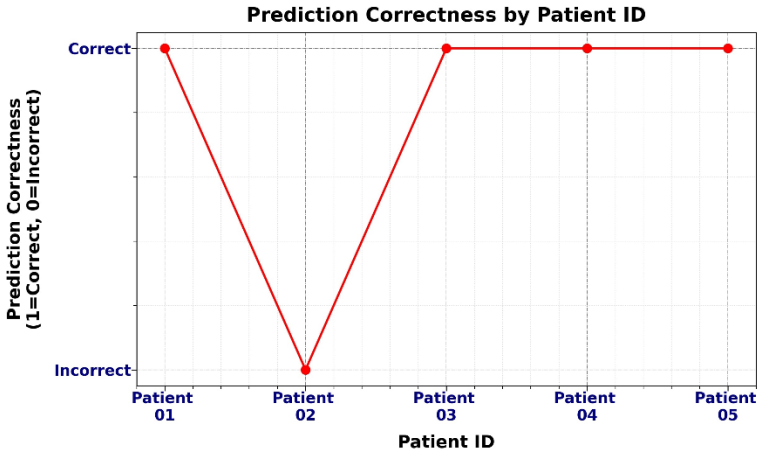

Figure 11.
The Prediction Correctness for Various Patients.

Figure 11 shows the prediction correctness for various patients identified by unique Patient IDs. Each patient, represented in order from Patient 01 to Patient 05, is assessed based on their

Edelweiss Applied Science and Technology
ISSN: 2576-8484
Vol. 9, No. 10: 189-211, 2025
DOI: 10.55214/2576-8484.v9i10.10383

corresponding predictions marked as either correct or incorrect. The values indicate that a "1" corresponds to a correct prediction, while a "0" signifies an incorrect one. The data highlights the performance of predictions made for each patient, allowing for comparison across multiple individuals. The predictive models perform with different patient data and identify patterns in accuracy or potential discrepancies in diagnosis or treatment outcomes. This enables a quick assessment of which patient IDs had better predictive correctness rates versus those needing improvement. This serves as an analytical tool to evaluate the efficiency of prediction within healthcare and encourages ongoing refinement of these predictive systems based on observed results across diverse patient scenarios.

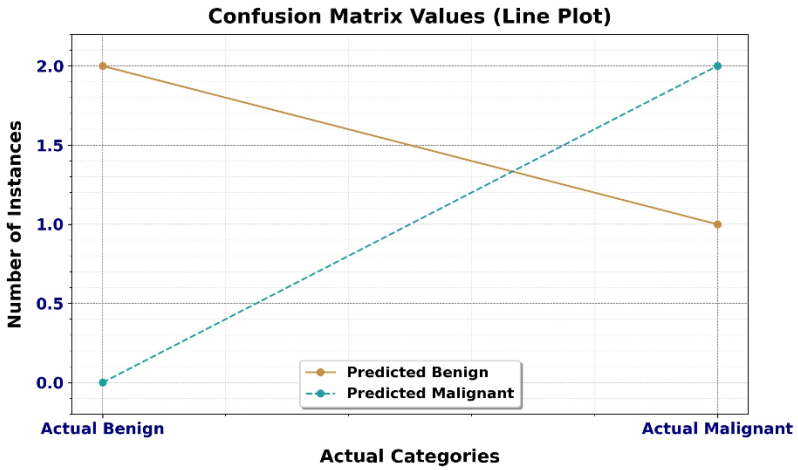

Figure 12.
Performance Metrics of a Classification Model.

Figure 12 shows the performance metrics of a classification model, specifically focusing on its confusion matrix values. The different predicted outcomes are benign and malignant instances. The range of values varies from 0.0 to 2.0, indicating the number of instances classified within each category. The increase towards a higher value signifies an increase in correctly identified cases, while the other contrasting trend is based on the predictions made by the model versus actual results. This comparison between actual categories determines how well the model performs in classifying benign and malignant instances. The insights into model accuracy help users understand areas where improvements may be needed or where predictive capabilities are strong. From the values in relation to actual occurrences, stakeholders can glean valuable information regarding efficacy and potential adjustments necessary for enhancing predictive performance in future assessments.

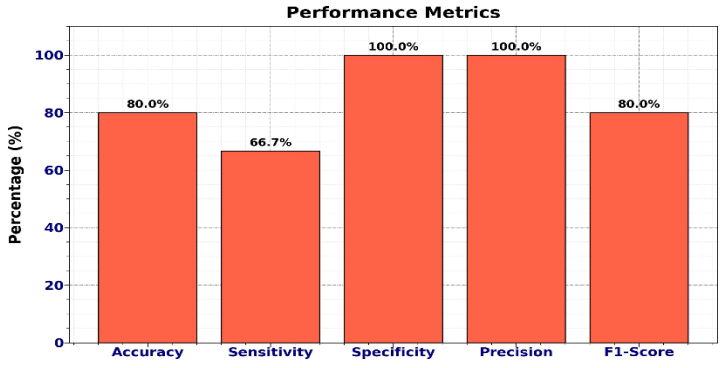

Figure 13.
Performance Metrics Percentage.

Edelweiss Applied Science and Technology
ISSN: 2576-8484
Vol. 9, No. 10: 189-211, 2025
DOI: 10.55214/2576-8484.v9i10.10383

Figure 13 illustrates various performance metrics, showcasing four key measurements: Accuracy, Sensitivity, Specificity, Precision, and F1-Score. The heights of the corresponding numerical values for each metric are on a percentage scale. The highest value displayed is 100%, indicating optimal performance in accuracy, and 80% in sensitivity and specificity. The chart also shows the F1-score with a value of 66.7%. The evaluating model's effectiveness: accuracy reflects overall correctness; sensitivity measures true positive rates; specificity assesses true negative rates; precision indicates the proportion of correct identifications; and the F1-score provides a balance between precision and recall. This allows for easy comparison across these critical performance indicators.

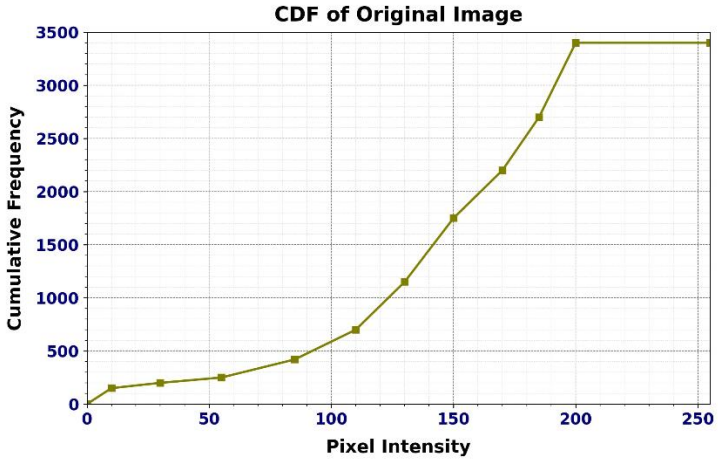

Figure 14.
Cumulative Distribution Function (CDF) of the Original Image.

Figure 14 shows the cumulative distribution function (CDF) of an original image. The relationship between pixel intensity and cumulative frequency is depicted. The pixel intensity values range from 0 to 250, indicating different levels of brightness or colour in the image, while the cumulative frequency ranges from 0 to 3500. The data indicates how frequently each pixel intensity occurs within the original image, allowing for an understanding of the brightness distribution. Values are prominently displayed at intervals to help quantify these aspects across both axes clearly. The pixel data in images highlights important statistical measures that are crucial for tasks such as image enhancement.

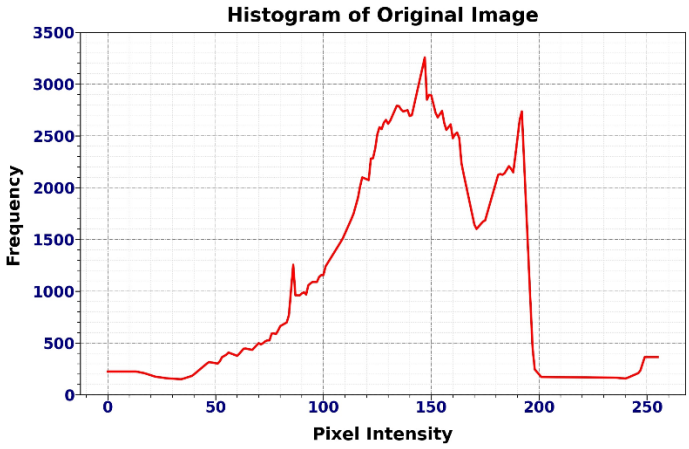

Figure 15.
Distribution of Pixel Intensities.

Edelweiss Applied Science and Technology
ISSN: 2576-8484
Vol. 9, No. 10: 189-211, 2025
DOI: 10.55214/2576-8484.v9i10.10383

Figure 15 represents the distribution of pixel intensities in an original image. The frequency of various pixel intensity values ranges from 0 to 250. The specific pixel intensity levels, along with the corresponding frequency count for each intensity level, are highlighted. The values include a range starting from zero and reaching up to 3500 in frequency counts, indicating each intensity level. This type of analysis is useful for understanding the tonal quality and contrast within an image by revealing how often certain brightness levels appear in the image. It provides insight into image quality based on how concentrated or sparse certain pixel intensities are throughout the graphical representation. This analysis serves to quantify images and compare them with others based on their structural properties determined by pixel distribution frequencies across varying intensities.

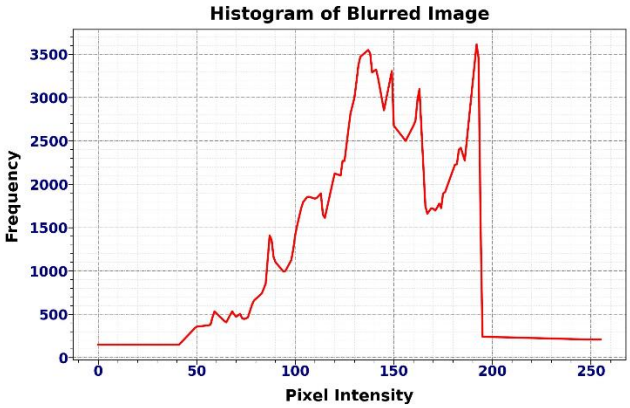

Figure 16.
Frequency Distribution of Pixel Intensity.

Figure 16 illustrates the frequency distribution of pixel intensity in a blurred image, providing insights into the tonal values present within it. The levels of pixel intensity range from 0 to 250, while the y-axis illustrates the corresponding frequency counts associated with these intensity levels. The specific intervals indicate which pixel intensities are more prevalent in the blurred image. The values reveal that at lower ranges of pixel intensity, there is a significant concentration of pixels highlighting lighter areas, while certain higher ranges display diminished frequency counts. This suggests a reduction of prominent darker tones within the distribution. The visual understanding of how light and dark elements coexist in the blurred image, while offering precise numerical data related to their frequencies. The essential information regarding how blurring affects visual content and its graduations within digital images.

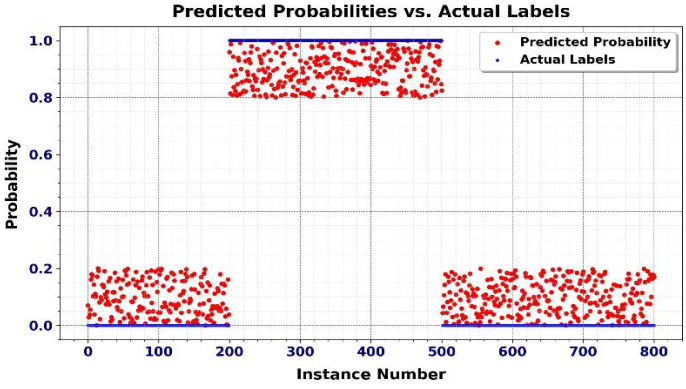

Figure 17.
Predicted Probabilities Vs. Actual Labels.

Edelweiss Applied Science and Technology
ISSN: 2576-8484
Vol. 9, No. 10: 189-211, 2025
DOI: 10.55214/2576-8484.v9i10.10383

Figure 17 shows two sets of points against a horizontal axis ranging from approximately 0 to 800. One set of points, representing predicted probabilities, is scattered across the vertical range of 0 to 1. These points appear concentrated in lower regions, generally below 0.2, and in a higher region, between 0.8 and 1.0. The other set of points, indicating actual labels, is distinctly positioned at values of 0 and 1 across the entire horizontal range. Specifically, these points form horizontal lines at the extreme bottom and top of the vertical axis. There are clear separations where the predicted probabilities tend to cluster and where the actual labels are definitively positioned. The vertical axis spans from 0 to 1, showing the scale for probability and labels. The arrangement of the plotted values allows for a visual comparison between the model's probability predictions and the true binary labels across different instances.

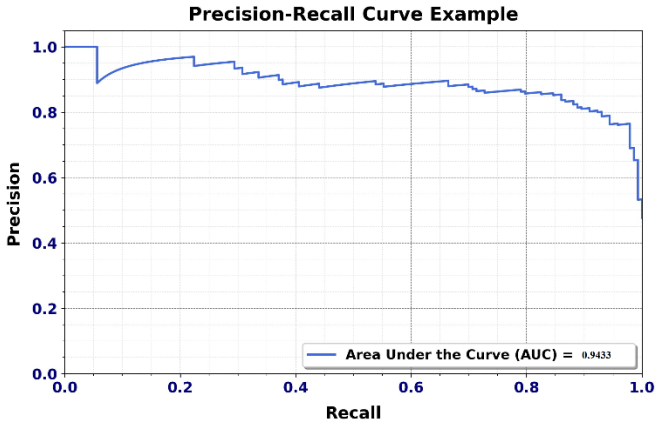

Figure 18.
Precision-Recall Curve Example.

Figure 18 displays a curve that begins at a vertical value of 1.0 and extends horizontally to a value of approximately 0.3. From this point, the curve gradually descends, showing fluctuations, and reaches a vertical value of around 0.3 at a horizontal value of 1.0. The horizontal axis ranges from 0.0 to 1.0, and the vertical axis also spans from 0.0 to 1.0. The plotted line illustrates a trend, whereas values along the horizontal dimension increase from 0 to 1, the corresponding values along the vertical dimension generally decrease from 1.0 to about 0.3, with some variations along the way. The area under this curve is quantified as approximately 0.9433. This plotted relationship showcases how one set of numerical values changes with respect to another across the specified range.

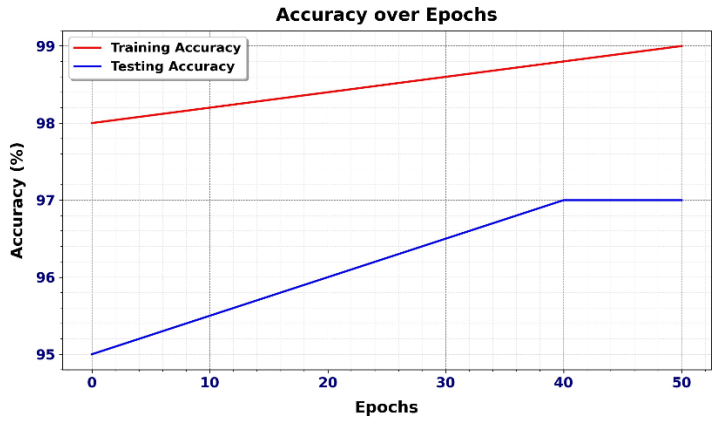

Figure 19.
Accuracy Over Epochs.

Edelweiss Applied Science and Technology
ISSN: 2576-8484
Vol. 9, No. 10: 189-211, 2025
DOI: 10.55214/2576-8484.v9i10.10383

Figure 19 illustrates two lines plotted against a shared horizontal axis ranging from 0 to 50. One line starts at a vertical value of 98 and gradually increases to approximately 99 over the entire horizontal range. The other line begins at a vertical value of 95 and increases to 97 around a horizontal value of 40, after which it remains constant at 97 until the end of the range. The vertical axis spans from 95 to 99. The progression of two distinct sets of values across the 50 units of the horizontal dimension is evident. One set of values shows a consistent upward trend, while the other exhibits an initial increase followed by a plateau. The specific numerical values at the start and end, as well as the point of change for the second set, are depicted.

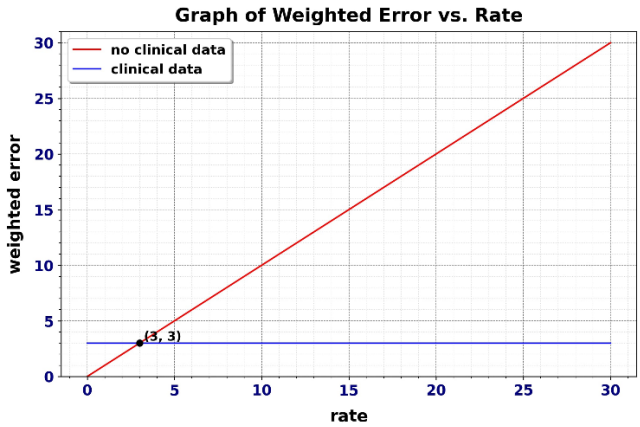

Figure 20.
Weighted Error in Clinical and Non-Clinical Data.

Figure 20 represents the clinical and non-clinical data in weighted error, with two lines plotted against a shared horizontal axis ranging from 0 to 30. One line starts at a vertical value of 0 and increases linearly to a value of 30 at the end of the horizontal range. The other line starts at a vertical value of approximately 3 and remains constant at this value across the entire horizontal range from 0 to 30. There is a point of intersection between the two lines at the horizontal value of 3 and the vertical value of 3. The vertical axis spans from 0 to 30. The plot illustrates two distinct trends: one where the value increases proportionally with the horizontal progression, and another where the numerical value stays stable across the entire horizontal span. The specific starting and ending values, as well as the point where the two trends meet, are presented.

Edelweiss Applied Science and Technology
ISSN: 2576-8484
Vol. 9, No. 10: 189-211, 2025
DOI: 10.55214/2576-8484.v9i10.10383

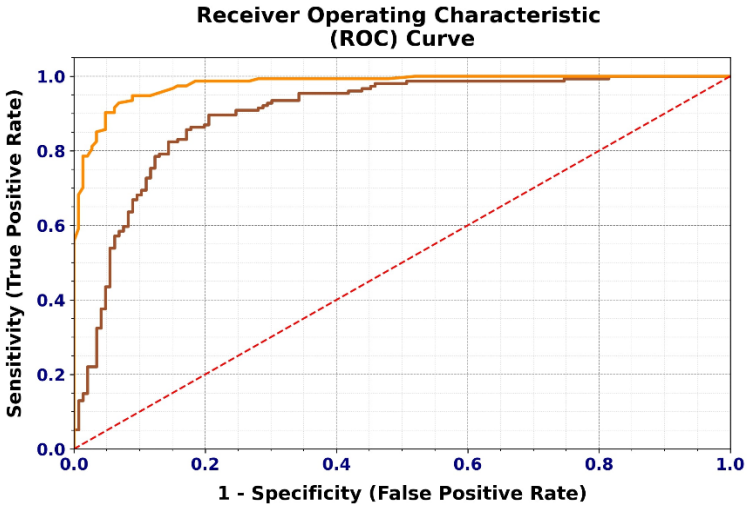

Figure 21.
Receiver Operating Characteristics (ROC) Curve.

Figure 21 shows the ROC curve in sensitivity and 1-specificity, two curves against a shared straight line ranging from 0.0 to 1.0. One curvature twitches at the origin (0.0, 0.0), rises sharply to a vertical value of approximately 0.95 at a horizontal value near 0.05, and then continues to increase gradually, reaching a vertical value of about 1.0 at a horizontal value of approximately 0.2. The second curve also twitches at the origin, increases to a vertical value of about 0.9 at a horizontal value of around 0.1, and then continues to rise gradually, reaching a vertical value close to 1.0 at a horizontal value of about 0.4. A dashed line spreads slantwise from the origin to the point (1.0, 1.0). The vertical axis ranges from 0.0 to 1.0. The relationship between the two sets of values shows how they change across the given range, with both tending towards a maximum vertical value as the horizontal value increases.

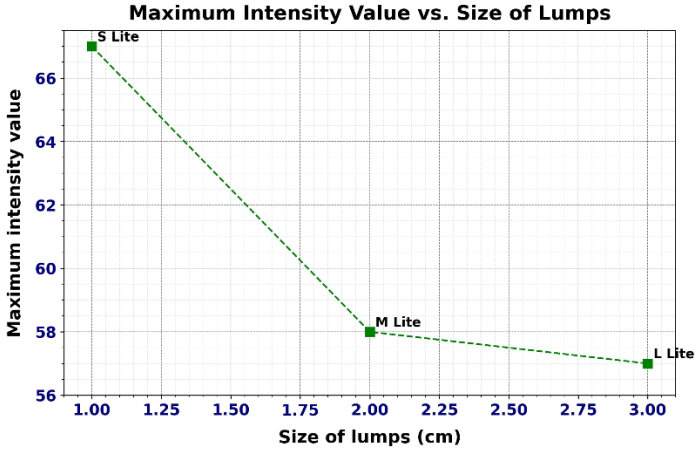

Figure 22.
Maximum Intensity Vs. Size of Lumps.

Figure 22 represents three distinct points connected by dashed lines. The horizontal axis ranges from 1.0 to 3.0. At a horizontal value of 1.0, there is a point with a vertical value of approximately 67. Another point is located at a horizontal value of 2.0, with a corresponding vertical value of about 58. The final point is at a horizontal value of 3.0, with a vertical value of approximately 57.5. The vertical axis spans from 57 to 67. The plot illustrates a decreasing trend in the vertical values as the horizontal

Edelweiss Applied Science and Technology
ISSN: 2576-8484
Vol. 9, No. 10: 189-211, 2025
DOI: 10.55214/2576-8484.v9i10.10383

values increase. Specifically, there is a significant drop from the first point to the second, followed by a smaller decrease from the second to the third. The numerical values at each of the three plotted locations are indicated by their positions on the two axes.

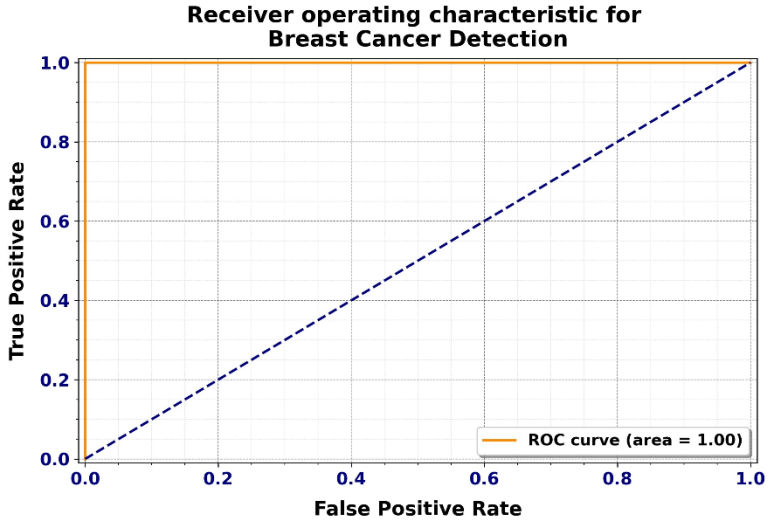

Figure 23.
Receiver Operating Characteristics for Breast Cancer Discovery.

Figure 23 shows the receiver operating characteristics for breast cancer discovery. The curve is plotted against a parallel axis ranging from 0.0 to 1.0. This curve starts at a vertical value of 1.0 and remains constant at this value across the entire horizontal range from 0.0 to 1.0. A diagonal from the origin (0.0, 0.0) to the point (1.0, 1.0). The axis also spans from 0.0 to 1.0. The area below the horizontal curve is quantified as 1.00. The ideal scenario is where one set of values remains at its maximum throughout the entire range of the other set of values. The cross-sectional line represents a baseline for comparison.

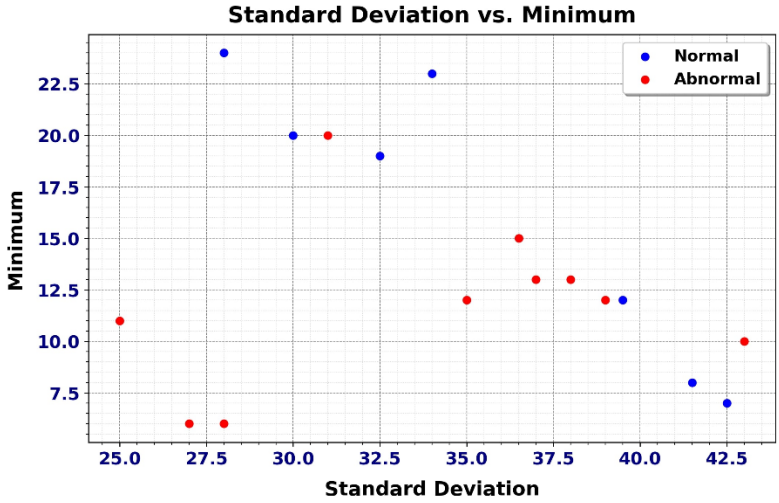

Figure 24.
Standard Deviation Vs. Minimum.

Edelweiss Applied Science and Technology
ISSN: 2576-8484
Vol. 9, No. 10: 189-211, 2025
DOI: 10.55214/2576-8484.v9i10.10383

Figure 24 displays two distinct sets of points. One set of points shows horizontal values ranging from approximately 28 to 43, with corresponding vertical values ranging from about 7 to 24. Specifically, some of these points are around (28, 24), (29, 20), (30, 24), (31, 24), (32, 19), (33, 14), (34, 23), (40, 10), (41.5, 8), and (43, 7). The other set of points has parallel values ranging from approximately 25 to 43, with corresponding erect values ranging from about 6 to 15. The horizontal axis spans from 25 to 45, and the vertical axis ranges from 5 to 25. The distinction between the two groups of data points is based on their straight and erect values.

5. Research Conclusion

ThermoFusionNet presents a novel and effective deep learning-based solution for the early discovery of breast irregularities by integrating both graphic and ultraviolet thermal imaging. The strengths of each imaging type are thermal imaging's ability to detect temperature anomalies associated with abnormal tissue growth and visual imaging's structural clarity to improve analytic correctness. The fusion of these modalities through a tailored CNN framework enables the system to learn and interpret complex patterns that may not be apparent in single-modality systems. Experimental results demonstrated that ThermoFusionNet achieved higher performance in key evaluation metrics, such as correctness, accuracy, recall, and F1-score, outperforming traditional and unimodal models. The results also showed reduced false positives and improved sensitivity to subtle abnormalities, highlighting the potential of the system for real-world clinical application. This research confirms that combining deep learning with imaging can significantly improve the dependability and competence of breast abnormality detection. ThermoFusionNet holds promise not only for aiding radiologists in early and accurate diagnosis but also for being implemented in low-resource settings due to the non-invasive and radiation-free nature of thermal imaging. Future work may focus on expanding datasets, real-time applications, and refining the model for broader use in other medical imaging fields, ensuring even greater diagnostic support and patient care.

Transparency:

The authors confirm that the manuscript is an honest, accurate, and transparent account of the study; that no vital features of the study have been omitted; and that any discrepancies from the study as planned have been explained. This study followed all ethical practices during writing.

Copyright:

References

[1] S. Harjasdeep and S. Durgesh, "Sentiment analysis: Quantitative evaluation of machine learning algorithms," in *Proceedings of the 5th International Conference on Smart Systems and Inventive Technology*, 2025.

[2] N. P. Patil and R. J. Ramteke, "A novel optimized deep learning framework to spot keywords and query matching process in Devanagari scripts," *Multimedia Tools and Applications*, vol. 82, no. 19, pp. 30177-30199, 2023. https://doi.org/10.1007/s11042-023-14912-1

[3] H. Vishal Sharad, S. R. Desai, and K. Y. Krishnrao, "Fault-tolerant multi-path data communication mechanism in WSN based on optimization enabled routing," *Wireless Personal Communications*, vol. 125, pp. 841-859, 2022. https://doi.org/10.1007/s11277-022-09580-7

[4] H. Vishal Sharad, S. R. Desai, and K. Y. Krishnrao, "Energy-aware multipath routing in WSN using improved invasive weed elephant herd optimization," *International Journal of Pervasive Computing and Communications*, vol. 19, no. 3, pp. 451-474, 2023. https://doi.org/10.1108/IJPCC-09-2021-0229

[5] S. Balshetwar and R. Tugnayat, "Framing and sentiment: Cumulative effect," in *2017 International Conference on Energy, Communication, Data Analytics and Soft Computing (ICECDS) (pp. 2873-2877). IEEE*, 2017.

[6] M. Khan, M. M. Su'ud, M. M. Alam, S. Karimullah, F. Shaik, and F. Subhan, "Enhancing breast cancer detection through optimized thermal image analysis using PRMS-Net deep learning approach," *Journal of Imaging Informatics in Medicine*, pp. 1-20, 2025. https://doi.org/10.1007/s10278-025-01465-y

[7] D. Youssef, H. Atef, S. Gamal, J. El-Azab, and T. Ismail, "Early breast cancer prediction using thermal images and hybrid feature extraction-based system," *IEEE Access*, vol. 13, pp. 29327-29339, 2025. https://doi.org/10.1109/ACCESS.2025.3541051

[8] A. Z. Nowakowski and M. Kaczmarek, "Artificial intelligence in IR thermal imaging and sensing for medical applications," *Sensors (Basel, Switzerland)*, vol. 25, no. 3, p. 891, 2025. https://doi.org/10.3390/s25030891

[9] T. Fan and W. Lin, "Deep learning-based thermal imaging analysis to diagnose abnormalities in sports buildings: Smart cyber-physical monitoring sensors at the edge," *Tsinghua Science and Technology*, vol. 30, no. 4, pp. 1457-1473, 2025. https://doi.org/10.26599/TST.2023.9010130

[10] T. E. Mousa, R. Zouari, M. Baklouti, M. Hamdi, and M. S. Geoda, "Deep learning methods for breast cancer detection and classification: A systematic review," *Journal of Engineering Science and Technology*, vol. 20, no. 1, pp. 209–234, 2025.

[11] S. Chaudhari, R. Gadakh, S. Mali, S. Govardhane, and S. Kale, "Detection of exudates of diabetic retinopathy using deep learning algorithms," *Open Access International Journal of Science and Engineering*, vol. 8, no. 3, pp. 43-46, 2025.

[12] N. Y. Duodu, W. D. Patel, and H. Koyuncu, "Advancements in telehealth: Enhancing breast cancer detection and health automation through smart integration of iot and cnn deep learning in residential and healthcare settings," *Journal of Advanced Research in Applied Sciences and Engineering Technology*, vol. 45, no. 2, pp. 214-226, 2025.

[13] M. Sudhi, D. K. Shetty, J. M. Balakrishnan, D. R. Prabhu, R. Kamath, and S. Girisha, "Thermal imaging applications in shock detection: Technological advancements and clinical implications," *Engineered Science*, vol. 33, p. 1367, 2025. https://doi.org/10.30919/es1367

[14] L. Garia and H. Muthusamy, "Dual-tree complex wavelet pooling and attention-based modified u-net architecture for automated breast thermogram segmentation and classification," *Journal of Imaging Informatics in Medicine*, vol. 38, pp. 887-901, 2025. https://doi.org/10.1007/s10278-024-01239-y

[15] C. Galazis, H. Wu, and I. Goryanin, "Breast cancer detection via multi-tiered self-contrastive learning in microwave radiometric imaging," *Diagnostics*, vol. 15, no. 5, p. 549, 2025. https://doi.org/10.3390/diagnostics15050549

[16] H. M. Rai, J. Yoo, S. Agarwal, and N. Agarwal, "LightweightUNet: Multimodal deep learning with GAN-augmented imaging data for efficient breast cancer detection," *Bioengineering*, vol. 12, no. 1, p. 73, 2025. https://doi.org/10.3390/bioengineering12010073

[17] F. J. Alvarez-Padilla, M. V. Argudin-Ferran, J. L. Flores-Nunez, and J. R. Alvarez-Padilla, "GuideNet: Leveraging UNet as Guidance for Anatomical Landmark-Based Breast Segmentation in Thermograms," 2025.

[18] H. R. Saeidnia, C. Sparks, and H. Soleymani Majd, "Conceptual model for breast cancer diagnosis using machine learning on mammogram data," *InfoScience Trends*, vol. 2, no. 3, pp. 11-26, 2025. https://doi.org/10.61186/ist.202502.02.02

[19] G. Wang, Z. Li, G. Weng, and Y. Chen, "An overview of industrial image segmentation using deep learning models," *Intelligence & Robotics*, vol. 5, no. 1, pp. 143-180, 2025. http://dx.doi.org/10.20517/ir.2025.09

[20] A. Piana, "Thermography in breast cancer detection: Identifying aggressive cancers and reducing overdiagnosis. Professional Academy of Clinical Thermology," 2025. https://medicalthermology.org/

[21] M. Pouriayevali, R. McWilliams, A. Bachar, P. Atwal, R. Ramaseshan, and F. Golnaraghi, "Advancing near-infrared probes for enhanced breast cancer assessment," *Sensors*, vol. 25, no. 3, p. 983, 2025. https://doi.org/10.3390/s25030983

[22] H. Edmonds, S. S. Mukherjee, B. Holcombe, K. Yeh, R. Bhargava, and A. Ghosh, "A machine learning-based approach for quantification of protein secondary structures from discrete frequency infrared images," *bioRxiv*, 2025. https://doi.org/10.1101/2025.01.08.632028

[23] T. E. Moradi and A. Rezai, "High-performance breast cancer diagnosis method using a hybrid feature selection method," *Biomedical Engineering / Biomedizinische Technik*, vol. 70, no. 2, pp. 171-181, 2025.

[24] J. Sun *et al.*, "A deep learning model based on chest CT to predict benign and malignant breast masses and axillary lymph node metastasis," *Biomolecules and Biomedicine*, vol. 26, no. 1, pp. 91-99, 2025. https://doi.org/10.17305/bb.2025.12010

[25] R. Jalloul, C. H. Krishnappa, V. I. Agughasi, and R. Alkhatib, "Enhancing early breast cancer detection with infrared thermography: a comparative evaluation of deep learning and machine learning models," *Technologies*, vol. 13, no. 1, p. 7, 2024. https://doi.org/10.3390/technologies13010007

[26] M. A. S. Al Husaini, M. H. Habaebi, and M. R. Islam, "Real-time thermography for breast cancer detection with deep learning," *Discover Artificial Intelligence*, vol. 4, p. 57, 2024. https://doi.org/10.1007/s44163-024-00157-w

[27] K. S. Ahmed, F. F. Sherif, M. S. Abdallah, Y.-I. Cho, and S. M. ElMetwally, "An innovative thermal imaging prototype for precise breast cancer detection: Integrating compression techniques and classification methods," *Bioengineering*, vol. 11, no. 8, p. 764, 2024. https://doi.org/10.3390/bioengineering11080764

[28] Y. Mirasbekov *et al.*, "Fully interpretable deep learning model using IR thermal images for possible breast cancer cases," *Biomimetics*, vol. 9, no. 10, p. 609, 2024. https://doi.org/10.3390/biomimetics9100609

[29] Z. Khomsi, M. Elfezazi, and L. Bellarbi, "Deep learning-based approach in surface thermography for inverse estimation of breast tumor size," *Scientific African*, vol. 23, p. e01987, 2024. https://doi.org/10.1016/j.sciaf.2023.e01987

[30] A. Y. Bani Ahmad, J. A. Alzubi, M. Vasanthan, S. B. Kondaveeti, J. Shreyas, and T. P. Priyanka, "Efficient hybrid heuristic adopted deep learning framework for diagnosing breast cancer using thermography images," *Scientific Reports*, vol. 15, p. 13605, 2025. https://doi.org/10.1038/s41598-025-96827-5

[31] S. Pechkova, L. Venger, D. Andonovski, and B. Andonovic, "Breast cancer detection from thermal images using machine learning," *ENTRENOVA-ENTerprise REsearch InNOVAtion*, vol. 10, no. 1, pp. 567-577, 2024. https://doi.org/10.54820/entrenova-2024-0042

[32] E. K. Ukiwe, S. A. Adeshina, T. Jacob, and B. B. Adetokun, "Deep learning model for detection of hotspots using infrared thermographic images of electrical installations," *Journal of Electrical Systems and Information Technology*, vol. 11, p. 24, 2024. https://doi.org/10.1186/s43067-024-00148-y

[33] A. Munguía-Siu, I. Vergara, and J. H. Espinoza-Rodríguez, "The use of hybrid CNN-RNN deep learning models to discriminate tumor tissue in dynamic breast thermography," *Journal of Imaging*, vol. 10, no. 12, p. 329, 2024. https://doi.org/10.3390/jimaging10120329

Edelweiss Applied Science and Technology
ISSN: 2576-8484
Vol. 9, No. 10: 189-211, 2025
DOI: 10.55214/2576-8484.v9i10.10383